Energy Storage Materials 65 (2024) 103154

Contents lists available at ScienceDirect

Energy Storage Materials

journal homepage: www.elsevier.com/locate/ensm

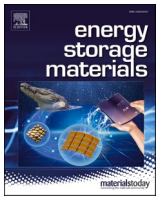

Microwave heating enables near-carbonless liquid-phase-derived Li Argyrodites for all-solid-state batteries

Boyeong Jang [1], Jehoon Woo [1], Yong Bae Song, Hiram Kwak, Juhyoun Park, Jong Seok Kim, Haechannara Lim, Yoon Seok Jung [*]

Department of Chemical and Biomolecular Engineering, Yonsei University, Seoul, 03722, Republic of Korea

ARTICLE INFO

Keywords:
Solid-state batteries
Solid electrolytes
Sulfides
Liquid-phase syntheses
Microwaves

ABSTRACT

The liquid-phase synthesis of sulfide solid electrolytes (SEs) is promising for the mass production of practical all-solid-state batteries (ASSBs). However, upon conventional furnace-based heat treatment of liquid-phase-derived intermediates, SEs contain deleterious carbon impurities from organic residues, negatively impacting the electrochemical performance of ASSBs and hindering their practical application. Herein, we present a novel approach utilizing ultrafast targeted heating through microwave-induced thermal shock, demonstrating the enhanced crystallization of SEs while effectively suppressing the carbonization of organic impurities during the liquid-phase synthesis of argyrodite SEs. Complementary analyses confirm the reduced sulfur loss and minimized impurity evolution achieved through microwave heating, as compared to conventional furnace heating. The microwave-derived argyrodite SEs exhibit high Li conductivities ($Li_{5.5}PS_{4.5}Cl_{1.5}$: maximum 3.1 mS cm^{-1}) and acceptably low electronic conductivities (Li_6PS_5Cl: 1.2 × 10^{-9} S cm^{-1}), in stark contrast to the mixed conducting property of furnace-derived Li_6PS_5Cl (Li^+ conductivity: 1.1 mS cm^{-1}, electronic conductivity: 1.7 × 10^{-5} S cm^{-1}). As a result, when utilized as SE layers or catholytes in $LiNi_{0.70}Co_{0.15}Mn_{0.15}O_2$||Li-In ASSB cells, the cells incorporating microwave-derived SEs significantly outperform those with furnace-derived SEs (e.g., the capacity retention after 250 cycles: 93.6% vs. 32.0%). Furthermore, a proof-of-concept for microwave self-heating of SEs is successfully demonstrated.

1. Introduction

Inorganic solid electrolytes (SEs) play a pivotal role in the realization of all-solid-state batteries (ASSBs) exhibiting high energy density and allowing enhanced safety, as opposed to conventional lithium-ion batteries that utilize flammable organic liquid electrolytes [1–5]. Within the diverse range of SE candidates, including sulfides, oxides, halides, and hydrides, sulfide materials stand out because of their exceptional ionic conductivities rivaling those of liquid electrolytes, and deformability, facilitating the scalable cold-pressing production of ASSBs [6–16].

In particular, argyrodite-type SEs (e.g., $Li_{6-x}PS_{5-x}Cl_{1+x}$ ($0 \leq x \leq 0.5$)) show multiple advantageous characteristics: [17–24] i) high ionic conductivities ranging from 10^{-3} to 10^{-2} S cm^{-1}; ii) absence of rare or costly constituent elements; iii) a crystalline structure guaranteeing consistent quality and properties, making them well suited for mass production; and iv) ability to undergo liquid-phase synthesis or processing.

Although solid-state synthesis is widely employed for the majority of inorganic SEs, liquid-phase synthesis or processing of sulfide SEs offers potential benefits in mass production, including shorter synthesis time, reduced energy consumption, and improved product homogeneity [11,12,18,19,25,26]. Moreover, liquid-phase syntheses can offer unique characteristics that are typically not observed in solid-state syntheses, such as the generation of metastable phases, varied morphologies, fine particles, enhanced deformability, and increased air stability [11,12,25,27-30].

For the liquid-phase synthesis of sulfide SEs, the precursors are mixed with solvents to form suspensions or solutions, which are then subjected to solvent evaporation. Subsequently, a heat treatment (HT) process is conducted to complete the synthesis. Argyrodites such as Li_6PS_5Cl (LPSCl) can be synthesized using two precursor solutions: a

* Corresponding author.
E-mail address: yoonsjung@yonsei.ac.kr (Y.S. Jung).
[1] These authors contributed equally.

https://doi.org/10.1016/j.ensm.2023.103154
Received 10 September 2023; Received in revised form 11 December 2023; Accepted 21 December 2023
Available online 21 December 2023

mixture of Li_2S and P_2S_5 in tetrahydrofuran (THF), and Li_2S and LiCl in ethanol (EtOH). After mixing the two solutions, the solvents are evaporated, and subsequent HT at 550 °C results in the formation of LPSCl [18,19]. However, complete removal of the solvents is challenging. Residual solvents can lead to the formation of impurity phases, which, in turn, reduce the ionic conductivity [31,32]. Furthermore, when subjected to high HT temperatures (e.g., conditions required for the generation of the argyrodite phase, such as 550 °C), chronic carbonization can occur. The resulting carbon impurities in the liquid-phase synthesized SEs can increase electronic conductivity, promoting side reactions or leakage currents in ASSB cells [33,34]. This issue may provide an explanation for the scarcity of literature demonstrating successful implementation of 4 V-class ASSB cells using liquid-phase-derived SEs (Table S1) [18,19,33,35-38].

In recent years, cutting-edge synthesis methods capable of rapidly producing inorganic materials have emerged, including microwave, Joule heating, plasma, flame, and laser synthesis techniques [39–42]. These methods release energy directly at targeted locations and offer significantly more efficient alternatives than conventional methods that rely on heat transfer (e.g., conduction, radiation, and convection). The ultrafast heating process minimizes the time for side reactions, resulting in the production of purer products [39]. Among these ultrafast synthesis methods, microwaves are particularly appealing because they selectively and directly heat materials based on their dielectric properties, making upscaling feasible [43,44]. However, there are only a limited number of studies on microwave-assisted synthesis for SE applications, especially those involving sulfide SEs [45–48].

Herein, we demonstrate, for the first time, that ultrafast microwave heating significantly suppresses the carbonization of organic impurities in liquid-phase-derived argyrodite SEs, resulting in near-carbonless products. Instant high-temperature heating up to ≈1000 °C was achieved via carbothermal shock by the microwave irradiation of LPSCl buried in carbon powders. LPSCl prepared using microwave heating exhibited higher Li^+ conductivities and significantly lower electronic conductivities than that prepared via conventional furnace heating. Substantially enhanced phase purity, particularly in terms of carbon impurities, was confirmed through complementary analyses including X-ray diffraction (XRD), solid-state ^{31}P magic-angle spinning nuclear magnetic resonance (MAS-NMR) spectroscopy, Raman spectroscopy, X-ray photoelectron spectroscopy (XPS), and elemental analysis. Finally, in ASSB cells, $LiNi_{0.7}Co_{0.15}Mn_{0.15}O_2$ (NCM) electrodes employing microwave-heated LPSCl outperformed those employing furnace-heated LPSCl in terms of initial Coulombic efficiency (ICE), capacity, rate capability, cycling performance, and leakage currents.

2. Results and discussions

Fig. 1a illustrates the application of microwave heating in the HT process during the liquid-phase synthesis of LPSCl. The liquid-phase reaction involved the mixing of Li_2S and P_2S_5 in THF, and separately, Li_2S and LiCl in EtOH. After the solvents were evaporated under a vacuum at a mild temperature of 200 °C, low-crystalline LPSCl SEs (hereafter referred to as "lc-LPSCl") were obtained. Subsequently, the lc-LPSCl pellet was covered with carbon powders and underwent microwave heating to induce the crystallization of the SEs. This process, known as microwave-induced carbothermal shock, enables the rapid heating of carbon materials owing to their dielectric properties when exposed to microwave radiation [40,46,47,49]. The ultrafast nature of this process can address a critical drawback of the liquid-phase synthesis of SEs by effectively suppressing the chronic carbonization of organic residues, which is discussed later. To accurately monitor the temperature changes within the carbon, an IR sensor was inserted through the top hole of the household microwave oven, as depicted in Fig. 1b. Fig. 1c presents the temperature profile of the carbon measured at different power levels (100 and 180 W), demonstrating rapid increases up to 600 and 1000 °C at 100 W and 180 W, respectively, within a few seconds during each pulse. Figure S1 provides photographs of the liquid-phase suspension, which is a mixture of two solutions: Li_2S and P_2S_5 in THF, and Li_2S and LiCl in EtOH, as well as the resulting dried lc-LPSCl. It also shows the setup for microwave heating, which consisted of an lc-LPSCl pellet embedded in carbon powder within a vacuum-sealed quartz tube.

The lc-LPSCl samples with two different compositions, Li_6PS_5Cl and

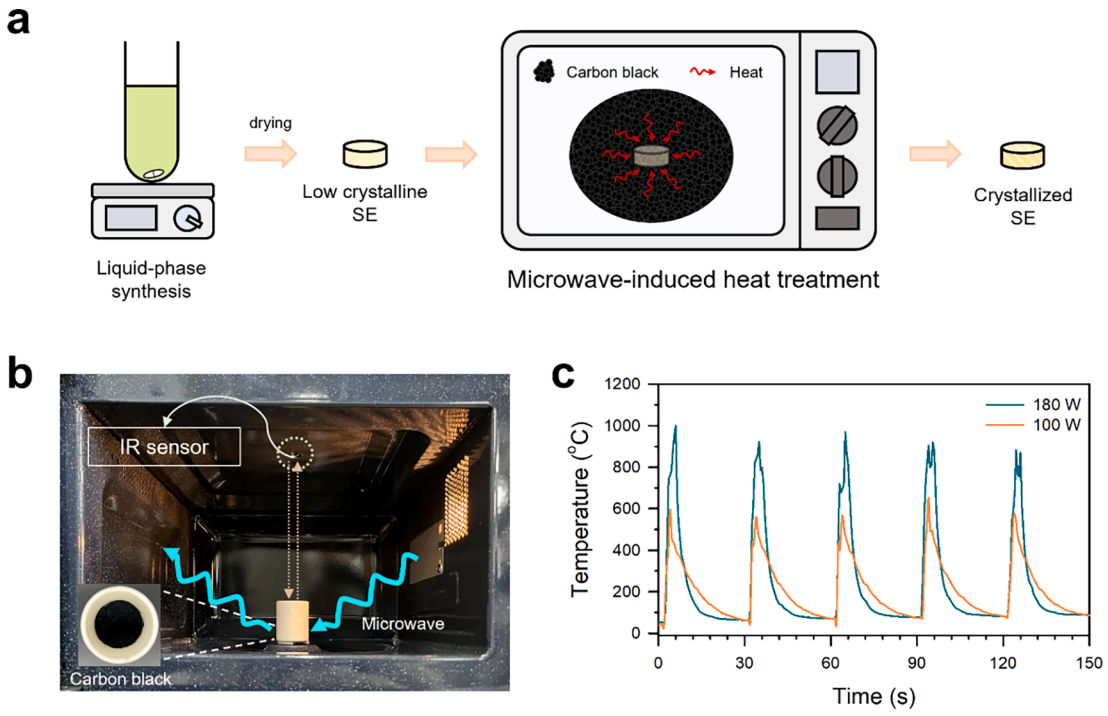

Fig. 1. Microwave heating for sulfide SE synthesis. (a) Schematic of the liquid-phase synthesis of argyrodite SEs via microwave heat treatment. (b) Photograph of the experimental setup employed to measure the temperature of carbon black during microwave irradiation. (c) Temperature profile of carbon black during pulsed microwave irradiation at 100 W and 180 W.

$Li_{5.5}PS_{4.5}Cl_{1.5}$, subjected to microwave heating are referred to as "MW-LPSCl" and "MW-LPSCl5.5," respectively. As a point of comparison, lc-LPSCl was conventionally heat-treated using a furnace at 550 °C for 6 h in an Ar atmosphere, with the resulting product referred to as "F-LPSCl". The scanning electron microscopy (SEM) images of F-LPSCl and MW-LPSCl powders are shown in Figure S2.

The Li^+ and electronic conductivities of the SE samples were measured using Ti|SE|Ti Li^+-blocking symmetric cells via AC and DC methods, respectively. Because of its high electronic conductivity, the Li^+ conductivity of F-LPSCl was determined by conducting electrochemical impedance spectroscopy (EIS) on electron-blocking and Li^+-nonblocking Li|LPSCl|F-LPSCl|LPSCl|Li symmetric cells (Figure S3, see the Experimental Section for more details) [33,50]. The results for lc-LPSCl, F-LPSCl, MW-LPSCl, and MW-LPSCl5.5 are displayed in Fig. 2a. The Arrhenius plots of the Li^+ conductivity for MW-LPSCl are shown in Figure S4. The XRD analysis of MW-LPSCl samples, subjected to various heating durations ranging from 0.5 to 15.0 min, revealed a marked increase in crystallinity after just 2 min (Figure S5). Consequently, the optimal HT conditions for achieving the highest ionic conductivity in MW-LPSCl and MW-LPSCl5.5 were established as 180 W for 5 and 3 min, respectively, as detailed in Table 1. The Li^+ conductivities of lc-LPSCl, F-LPSCl, MW-LPSCl, and MW-LPSCl5.5 were 0.12, 1.0, 2.5, and 3.1 mS cm^{-1} at 30 °C. Notably, the Li^+ conductivity of MW-LPSCl was higher than that of F-LPSCl. More importantly, the microwave-derived LPSCl exhibited sufficiently low electronic conductivities (1.2×10^{-9} and 4.0×10^{-9} S cm^{-1} for MW-LPSCl and MW-LPSCl5.5, respectively), in stark contrast to the high value for conventional furnace-derived LPSCl (1.7×10^{-5} S cm^{-1}).

To examine the impact of various drying conditions prior to HT for furnace heating, control experiments were conducted, as outlined in Table 1. These experiments involved modifications to pre-drying and vacuum drying parameters (temperature and time), based on the current study and previous reports [19]. Corresponding XRD patterns and ionic/electronic conductivities of F-LPSCl samples are presented in Figures S6 and 2a, respectively. Under optimal conditions, the electronic conductivities of F-LPSCl were reduced, reaching 4.9×10^{-8} S cm^{-1} at the lowest (C4 in Table 1). However, this value remained significantly higher than those for MW-LPSCl samples (early 10^{-9} S cm^{-1}, Table 2). It is important to note that these low values could be achieved through

Table 1
Conditions of solvent drying process and heat treatment for lc-LPSCl, along with Li^+ and e^- conductivities of corresponding F-LPSCl samples.

Condition	Solvent drying		Heat treatment	Li^+ conductivity (mS cm^{-1})	e^- conductivity (S cm^{-1})
	Pre-drying[a]	Vacuum-drying	Atmosphere		
C1	Δ	200 °C, 6 h	Static vacuum	1.8	2.8×10^{-7}
C2	Δ	200 °C, 6 h	Ar flow	1.0	1.7×10^{-5}
C3	O	200 °C, 6 h	Static vacuum	2.0	3.9×10^{-6}
C4	O	200 °C, 6 h	Ar flow	0.6	4.9×10^{-8}
C5	O	140 °C, 20 h	Static vacuum	1.3	8.0×10^{-6}
C6	O	140 °C, 20 h	Ar flow	2.0	2.5×10^{-7}

[a] Vacuum drying process conducted at room temperature, continuing until samples reach a powdery form.

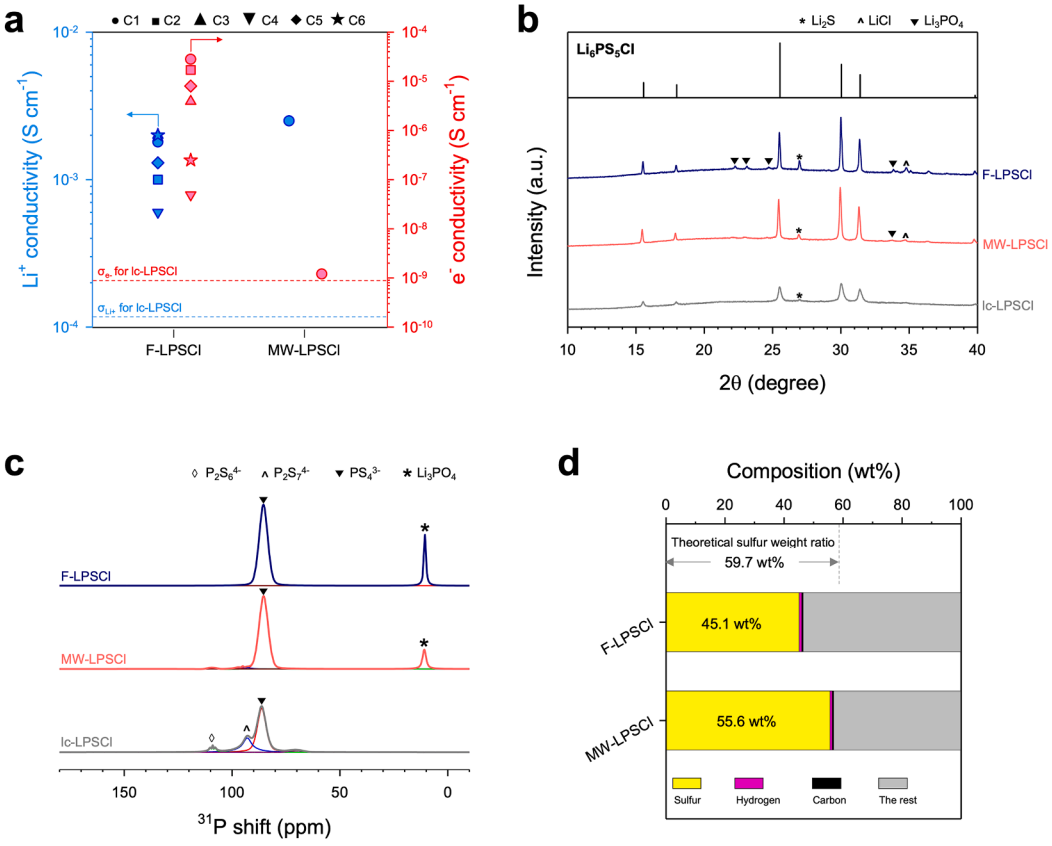

Fig. 2. Comparative characterization of LPSCl prepared by microwave and furnace heating. (a) Li^+ and e^- conductivities at 30 °C for F-LPSCl samples, prepared under various heat treatment conditions, and MW-LPSCl. The values for lc-LPSCl are also depicted as a horizontal dashed line. The specific conditions for each F-LPSCl sample are described in Table 1. (b) XRD patterns of lc-LPSCl, MW-LPSCl, and F-LPSCl. (c) ^{31}P MAS-NMR spectra of lc-LPSCl, MW-LPSCl, and F-LPSCl. (d) Elemental analysis results of F-LPSCl and MW-LPSCl.

Table 2
Li^+ and e^- conductivities of LPSCl and LPSCl5.5 prepared via microwave HT under different conditions.

Composition	Power (W)	Duration (min)	Li^+ conductivity (mS cm^{-1})	e^- conductivity (S cm^{-1})
Li_6PS_5Cl	100	3.0	0.21	1.0×10^{-9}
		5.0	0.37	1.2×10^{-9}
		10.0	1.0	1.3×10^{-9}
	180	0.5	0.23	4.0×10^{-10}
		1.0	0.25	8.5×10^{-10}
		1.5	0.83	1.7×10^{-9}
		2.0	1.6	4.7×10^{-9}
		3.0	1.8	1.7×10^{-9}
		5.0	2.5	1.2×10^{-9}
		7.0	1.8	1.8×10^{-8}
		15.0	2.0	1.2×10^{-8}
	300	0.5	0.20	4.9×10^{-10}
		1.5	2.1	7.5×10^{-8}
		3.0	1.1	1.1×10^{-5}
	450	0.5	1.9	1.9×10^{-8}
	700	0.5	2.0	2.8×10^{-7}
$Li_{5.5}PS_{4.5}Cl_{1.5}$	100	5.0	0.36	4.3×10^{-10}
		10.0	0.45	5.7×10^{-10}
	180	2.0	2.4	6.8×10^{-10}
		3.0	3.1	4.0×10^{-9}
		3.5	2.3	7.6×10^{-9}
		4.0	2.4	7.6×10^{-9}
		5.0	0.70	1.0×10^{-7}

microwave heating of lc-LPSCl, which was prepared under an unoptimized drying condition (C1 in Table 1). Such findings validate the superior efficacy of microwave heating in achieving crystallization of SEs without simultaneously increasing electronic conductivities.

Fig. 2b shows the powder XRD patterns of lc-LPSCl and LPSCl produced using two different HT methods (F-LPSCl and MW-LPSCl). Compared with lc-LPSCl, F-LPSCl exhibited sharper peaks, indicating increased crystallinity. However, consistent with previous findings, the evolution of impurity phases, including Li_2S, LiCl, and Li_3PO_4, is evident, which may arise from side reactions between LPSCl and organic residues and/or sulfur loss during the synthesis process [18,38]. Notably, the XRD patterns of MW-LPSCl show a similar level of crystallinity as that of F-LPSCl, with substantially lower impurity phase signals. Rietveld refinement of the XRD results confirmed the significantly lower amount of impurity phases in MW-LPSCl than in F-LPSCl (Figure S7 and Table S2). As a control experiment, lc-LPSCl was heat-treated in a furnace at 550 or 1000 °C for 5 min. However, this also yielded considerable amounts of impurities with insufficient crystallinity in the LPSCl phase, as revealed by the XRD results in Figure S8. Moreover, the resulting Li^+ conductivities were low: 0.32 and 0.88 mS cm^{-1} for the samples heat-treated at 550 and 1000 °C, respectively. In particular, the electronic conductivity of the sample heat-treated at 1000 °C for 5 min was as high as 1.3×10^{-4} S cm^{-1}.

The local environment of phosphorus in the LPSCl samples was probed using ^{31}P MAS-NMR spectroscopy, and the spectra of lc-LPSCl, F-LPSCl, and MW-LPSCl are shown in Fig. 2c. lc-LPSCl exhibited features of various P structural environments corresponding to $P_2S_8^{4-}$, $P_2S_7^{4-}$, and PS_4^{3-} [17,51,52]. Following the HT process using either a furnace or microwave, the P environments exhibited a convergence toward those corresponding to PS_4^{3-}, which is in good agreement with the crystal structure of Li_6PS_5Cl. Notably, F-LPSCl exhibited a significantly higher signal of Li_3PO_4 at ≈10 ppm compared to MW-LPSCl, which is consistent with the XRD results (Fig. 2b) [53]. It should also be noted that the HT conditions could affect the sublimation of sulfur [54], which guided us to conduct an elemental analysis. Surprisingly, the results reveal a substantial difference in the weight fraction of sulfur between F-LPSCl and MW-LPSCl (Fig. 2d). The sulfur content of MW-LPSCl (55.6 wt%) was highly consistent with the theoretical value (59.7 wt% for the pure phase of Li_6PS_5Cl), whereas F-LPSCl showed a significantly lower value of 45.1 wt%. This result indicates that conventional HT using a furnace results in severe sulfur loss, which can also contribute to the formation of impurity phases [51,55].

The high HT temperature, typically ≈550 °C, required for the synthesis of argyrodite SEs, is sufficient to carbonize residual organic species in liquid-phase-derived intermediates after drying (i.e., lc-LPSCl) [18,19,38]. The lc-LPSCl powders that were heat-treated in a furnace exhibited progressively darker features as the HT temperature increased (Figure S9 and Fig. 3a), indicating that significant carbonization occurs during the high-temperature HT processes. In contrast, microwave HT of lc-LPSCl resulted in pale gray powders similar to lc-LPSCl (Fig. 3a), signifying substantial suppression of carbonization in LPSCl.

The carbonization of SEs leads to an increase in electron conductivity, thereby transforming them into mixed conductors. Fig. 3b shows the Nyquist plots of F-LPSCl and MW-LPSCl in Ti|SE|Ti Li^+-blocking symmetric cells. MW-LPSCl displayed a steep and linear Warburg tail in the low-frequency region, starkly contrasting to F-LPSCl, which exhibited a tail curving downward to form an incomplete arc. This strongly indicates a significant electronic conductivity [36–38], as revealed by the measurement data shown in Fig. 2a. Raman spectroscopy was employed to assess the degree of carbonization (Fig. 3c). Because lc-LPSCl was obtained after the solvents were evaporated and dried at a low temperature of 200 °C, it did not exhibit any carbon signals [56]. Conversely, F-LPSCl exhibited prominent d- and G-band peaks at 1580–1350 cm^{-1} [56], confirming severe carbonization. In comparison, the peak intensities of MW-LPSCl were considerably lower. The peak areas of the d- and G-bands, normalized to those of PS_4^{3-} at 420 cm^{-1} for MW-LPSCl, were 4.9 times lower than those for F-LPSCl. Additionally, cyclic voltammetry (CV) tests using SE-C||Li-In cells at 30 °C revealed that F-LPSCl demonstrated higher redox currents than MW-LPSCl (Figure S10), suggesting that the increased presence of carbon impurities in LPSCl induced more electrochemical side reactions.

The microwave-heated LPSCl samples exhibited low electronic conductivities of $\leq \approx 10^{-9}$ S cm^{-1} (Table 2), making them suitable for separating SE layers. NCM|SE|Li-In all-solid-state half-cells using F-LPSCl or MW-LPSCl as SE layers were subjected to self-discharge tests, and the electrochemical results at 30 °C are displayed in Fig. 3d, e. Composite cathodes were prepared by manually mixing NCM, solid-state synthesized LPSCl, and super C65 at a weight ratio of 70:30:3. The open-circuit voltages (OCVs) of each half-cell were monitored for 400 h at 30 °C (Figure S11). The cell employing F-LPSCl with high electronic conductivity ($>10^{-5}$ S cm^{-1}) exhibited a rapid decrease in OCV during the initial period owing to leakage currents through the electronically conductive F-LPSCl layer. Additionally, without any resting period, the same cell was cycled once, charged to 4.3 V (vs. Li/Li^+) at 0.1C, and then kept at rest for 7 days at 30 °C before subsequent discharge. While the cell with F-LPSCl displays a distinct voltage decrease to 2.5 V (vs. Li/Li^+), the cell with MW-LPSCl shows a negligible change in voltage during storage (Fig. 3d). Fig. 3e shows the discharge voltage profiles of the cells with and without storage in the charged state during the 2nd cycle. The cells employing F-LPSCl experienced a significant loss in discharge capacity, reaching a 45 mA h g^{-1} reduction after only 3 days of storage. In a separate case, after 7 days of storage, these cells exhibited no capacity. In contrast, the cells with MW-LPSCl exhibited a considerably smaller loss in discharge capacity, with only 16 mA h g^{-1} reduction after 7 days of storage.

Furthermore, NCM711||Li-In all-solid-state half-cells employing F-LPSCl, MW-LPSCl, or MW-LPSCl5.5 as catholytes were cycled in the voltage range of 3.0–4.3 V (vs. Li/Li^+) at 30 °C, and the results are presented Fig. 4a-c. The solid-state-synthesized LPSCl was used as separating SE layers. The first-cycle charge-discharge voltage profiles at 0.1C are shown in Fig. 4a. The cells with MW-LPSCl and MW-LPSCl5.5 exhibited significantly higher reversible capacities (168 and 174 mA h g^{-1} vs. 144 mA h g^{-1}) and ICEs (77.0% and 77.5% vs. 67.9%, respectively) than those with F-LPSCl. Figs. 4b and S12 illustrate the rate capabilities of the CEs, further highlighting the superior performance in the following order: MW-LPSCl5.5 > MW-LPSCl >> F-LPSCl. Fig. 4c

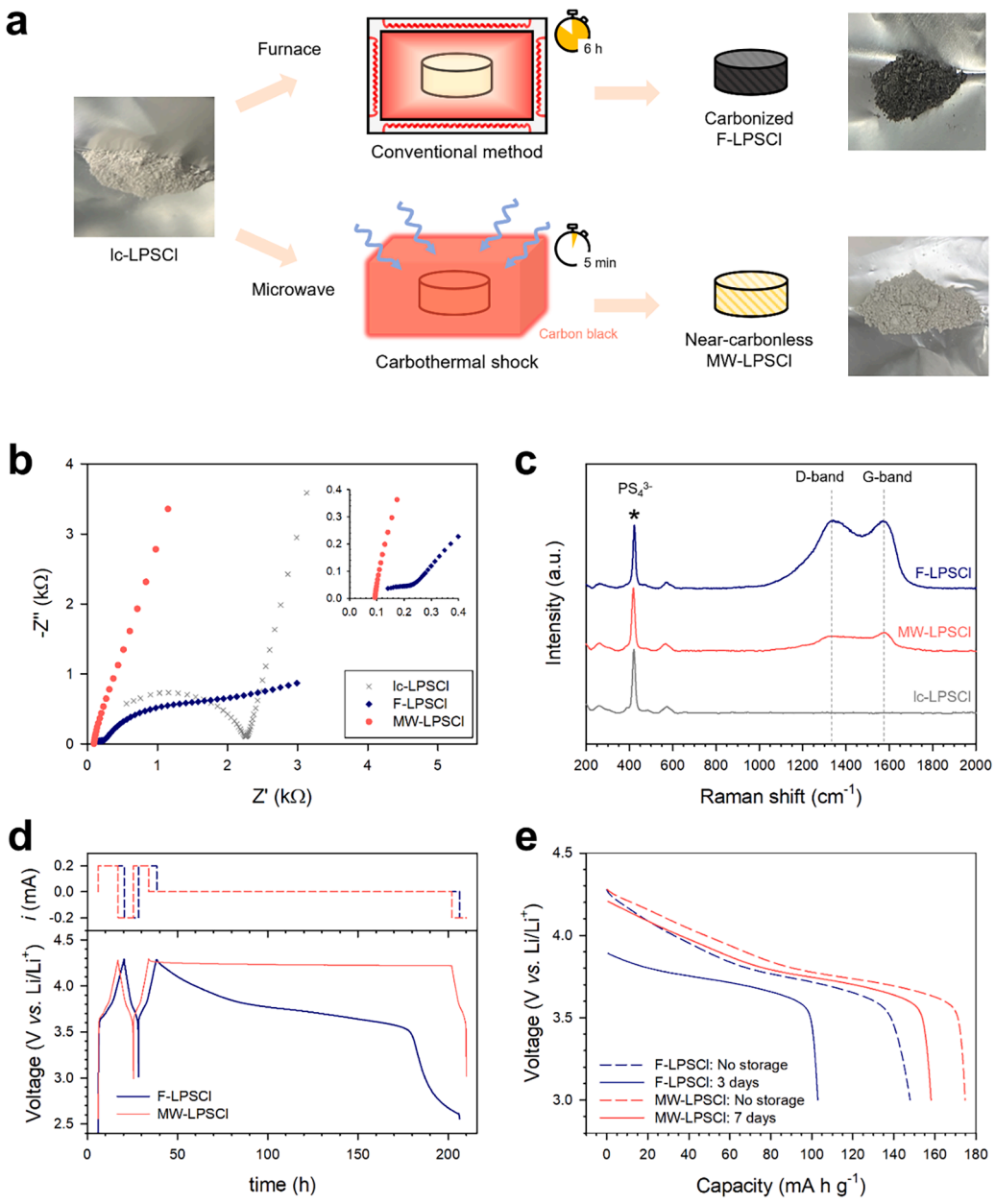

Fig. 3. Comparative evaluation of LPSCl prepared by microwave and furnace heating concerning carbon impurities. (a) Schematic comparing LPSCl preparation via furnace and microwave heating, including photographs of SE powders before and after the HTs. (b) Nyquist plot and (c) Raman spectra of lc-LPSCl, MW-LPSCl, and F-LPSCl. (d) Voltages of NCM||Li-In half-cells at 30 °C with F-LPSCl or MW-LPSCl as SE layers as a function of time and corresponding current during two cycles with storage for 7 days at 30 °C, followed by discharge. (e) Discharge voltage profiles of NCM||Li-In half-cells at 30 °C for using F-LPSCl and MW-LPSCl as SE layers, with variation of storage after initial charge at 30 °C.

shows the cycling performance with CEs at 0.5C. The capacity retentions of MW-LPSCl and MW-LPSCl5.5 were as high as 91.6% and 93.6%, respectively, in sharp contrast to 32.0% for F-LPSCl. This result can be attributed to the substantially reduced side reactions originating from the much lower amounts of carbon impurities in the microwave-derived LPSCls than F-LPSCl, as revealed from the CV results (Figure S10). Fig. 4d, e present the ex situ XPS results of the NCM electrodes employing F-LPSCl and MW-LPSCl after one cycle. After cycling, a noticeable increase in the signals of oxidative species, including bridging sulfur (P-$[S]_n$-P), P_2S_5, PO_4^{3-} and SO_4^{2-}, was observed, indicating the occurrence of side reactions [57–62]. These increases were considerably more pronounced for the electrodes using F-LPSCl compared to those using MW-LPSCl (Figs. 4d, e, S13, and Table S3).

Finally, Li|SE|Li symmetric cells employing F-LPSCl and MW-LPSCl were assessed at 30 °C (Figure S14). The fluctuating cycling voltage profiles for the cells with F-LPSCl contrasted with the stable profiles for the cells with MW-LPSCl, emphasizing the significance of carbon impurities in LPSCl.

This study used carbon as a microwave absorber to facilitate the heating of the SEs. However, in materials such as superionic conductors that contain mobile charge carriers, MW fields can generate currents that travel in phase with the field, resulting in heating [44,63]. In this context, SEs can function as microwave absorbers themselves. Regrettably, our attempt to achieve microwave-induced self-heating of LPSCl without a carbon material led to a thermal runaway. This can be attributed to the high ionic conductivity ($\geq 10^{-3}$ S cm^{-1}) of LPSCl, which causes the rapid conversion of microwaves into heat under normal conditions [44,63]. In contrast, microwave self-heating was achieved

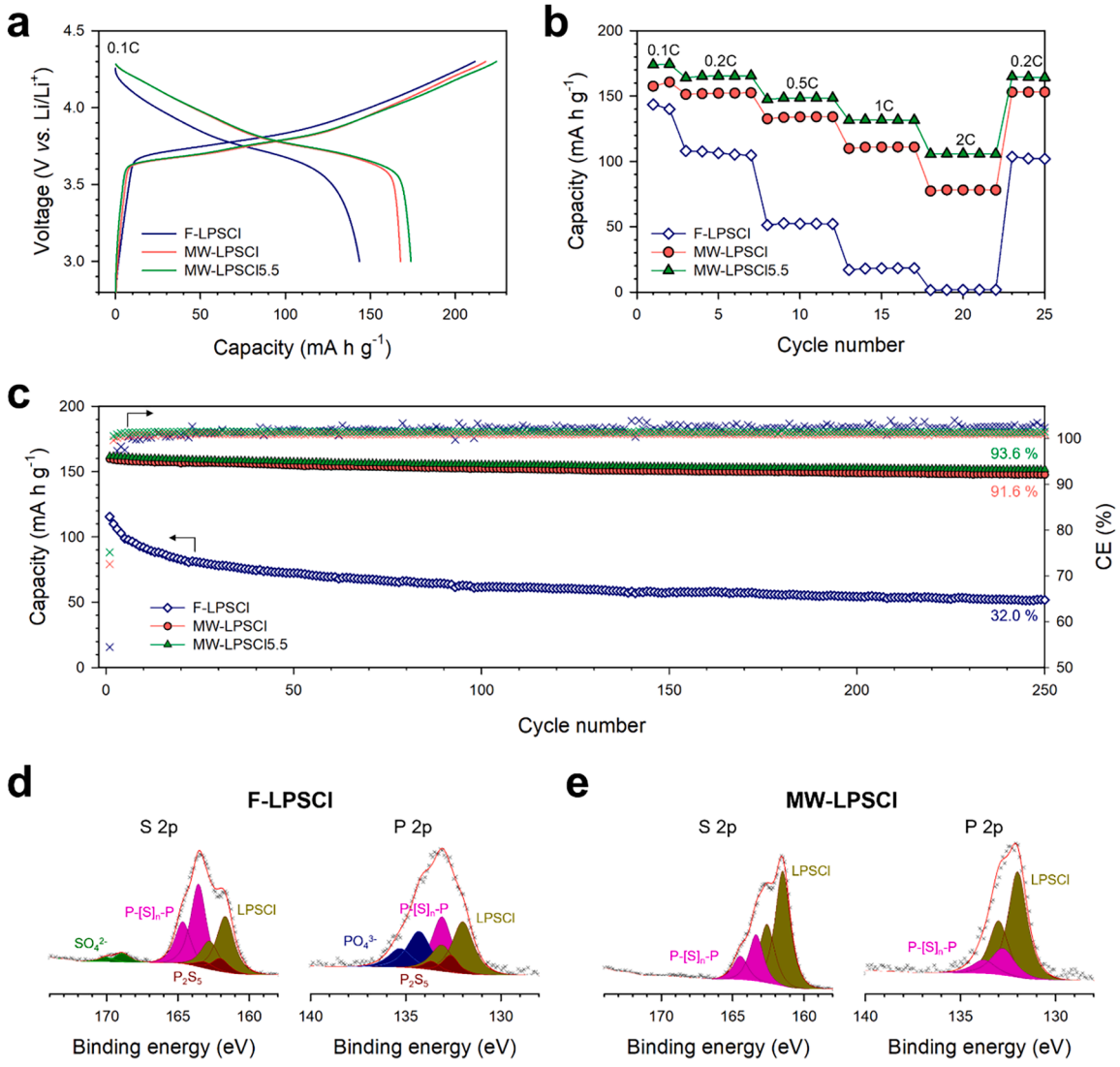

Fig. 4. Comparative electrochemical performance of the NCM electrodes employing F-LPSCl, MW-LPSCl, and MW-LPSCl5.5 as catholytes in NCM||Li-In all-solid-state half-cells at 30 °C. (a) First-cycle charge-discharge voltage profiles at 0.1C, (b) rate capability, and (c) cycling performance with CEs at 0.5C. Ex situ XPS spectra of S 2p and P 2p for the electrodes employing (d) F-LPSCl and (e) MW-LPSCl after one cycle.

using Li_6PS_5I (LPSI). We followed the liquid-phase synthesis protocol, which involved preparing low-crystalline LPSI by mixing solutions of Li_2S and P_2S_5 in THF, and Li_2S and LiI in EtOH, followed by solvent evaporation and vacuum drying at 200 °C (referred to as "lc-LPSI"). The resulting lc-LPSI exhibited a Li^+ conductivity of 0.1 mS cm^{-1}. When subjected to microwave heating at 700 W for 15 min without the presence of carbon, no thermal runaway occurred, yielding a product with improved XRD crystallinity (Figure S15) and demonstrating Li^+ and electronic conductivities of 6.5×10^{-6} S cm^{-1} at 30 °C and 7.5×10^{-10} S cm^{-1}, respectively (Figure S16) [17,21]. Surprisingly, when tested as a catholyte for NCM electrodes in NCM||Li-In all-solid-state half-cells at 30 °C, electrodes with microwave-derived LPSI significantly outperformed those with furnace-derived LPSI (first discharge capacity of 161 vs. 32 mA h g^{-1}, Figure S17), despite having comparable Li^+ conductivity (6.5×10^{-6} vs. 3.0×10^{-6} S cm^{-1}). This highlighted the purity of microwave-derived SEs. Based on these results, we believe that by controlling the MW heating conditions, such as power and time, it is possible to directly heat LPSCl without the need for auxiliary absorbers and prevent thermal runaway. This will be the focus of our next investigation.

3. Conclusion

Argyrodite SEs with high Li^+ conductivities (Li_6PS_5Cl: 2.5 mS cm^{-1}, $Li_{5.5}PS_{4.5}Cl_{1.5}$: 3.1 mS cm^{-1} at 30 °C) and sufficiently low electronic conductivities (Li_6PS_5Cl: 1.2×10^{-9} S cm^{-1}, $Li_{5.5}PS_{4.5}Cl_{1.5}$: 4.0×10^{-9} S cm^{-1}) were successfully prepared via a liquid-phase route using microwave-induced carbothermal shock HT. Ultrafast microwave heating in just a few minutes effectively inhibits the carbonization of organic residues in liquid-phase-derived intermediates. This starkly contrasts the severe carbonization (resulting in an electronic conductivity of 1.7 $\times 10^{-5}$ S cm^{-1}) and the corresponding impurity evolution observed in conventional furnace-based HTs. These findings were corroborated through complementary analyses using XRD, Raman spectroscopy, ^{31}P-NMR, XPS, elemental analysis, and electrochemical measurements. When applied to SE layers or catholytes in NCM||Li-In all-solid-state half-cells or SE layers in Li||Li symmetric cells, microwave-derived LPSCl significantly outperformed their furnace-derived counterparts in terms of self-discharge, capacity, CE, rate capability, and cycling performance. Furthermore, we successfully demonstrated a proof-of-concept for the microwave-induced self-heating of SEs and their implementation in ASSB cells by utilizing low-Li^+-conductive, liquid-phase-derived LPSI, thereby offering insights into the potential

optimization of LPSCl. This study is considered a significant breakthrough in the mass production of sulfide SE materials, potentially paving the way for the realization of practical large-scale ASSBs. Furthermore, our findings have the potential to serve as strong catalysts for future explorations in rapid production technologies for inorganic materials, spanning various disciplines.

4. Experimental section

4.1. Material preparation

LPSCl (Li_6PS_5Cl) powders were synthesized through a liquid-phase reaction by suspending a stoichiometric mixture of Li_2S (99.9%, Alfa Aesar) and P_2S_5 (99%, Sigma-Aldrich) in THF (99.9%, anhydrous, Sigma-Aldrich). The mixture was then stirred overnight at room temperature. The second solution was prepared using a stoichiometric mixture of Li_2S (99.9%, Alfa Aesar) and LiCl (99.99%, Alfa Aesar) in anhydrous EtOH. These two solutions (Li_2S and P_2S_5 in THF; Li_2S and LiCl in EtOH) were also stirred at room temperature overnight. The resulting solution was dried at 200 °C for 6 h under a vacuum to yield lc-LPSCl. For control experiments, several samples underwent pre-drying at room temperature under a vacuum until they reached a powdery form, as detailed in Table 1, before proceeding to the elevated-temperature drying process. To prepare F-LPSCl and MW-LPSCl, the lc-LPSCl pellet (150 mg), which was initially prepared at 370 MPa, was subjected to HT using a furnace and microwave, respectively. Furnace HT was conducted with an Ar flow at 550 °C for 6 h, using a heating rate of 5 °C min^{-1}. For the short-duration furnace heating, the sample was sealed in a quartz tube under an Ar flow and then placed inside a pre-heated furnace set to either 550 °C or 1000 °C. Subsequently, the sample was promptly removed after 5 min. The microwave-heated LPSCl samples were prepared in a standard household microwave oven, MS23M4033AG (Samsung). The lc-LPSCl pellet was embedded at the center of Super C65 (250 mg) in a quartz tube and sealed under a vacuum. Subsequently, the microwave HT was performed under various power and time conditions. The same liquid-phase process was employed to synthesize LPSI (Li_6PS_5I) powders through a furnace or microwave HT. The procedure involved two solutions: Li_2S and P_2S_5 in THF, and Li_2S and LiI in EtOH. To obtain F-LPSI, a similar process as that employed for F-LPSCl was conducted using a furnace. However, MW-LPSI was obtained without the inclusion of any microwave absorbers, such as carbon materials. Instead, the lc-LPSI powders were sealed within a glass ampoule under vacuum, and microwave HT was conducted at 700 W for 15 min.

4.2. Material characterization

Powder XRD patterns were obtained using a Rigaku MiniFlex600 with Cu-K_α radiation ($\lambda = 1.5406$ Å) at 40 kV and 15 mA. The samples were placed in airtight containers sealed with Be windows to avoid air exposure. The XRD patterns of a 50:50 wt ratio mixture of SE and ZnO were refined using the Rietveld refinement method with Fullprof software. The structural parameters of the ZnO crystal, used as reference material, and the SEs were obtained, allowing for the quantification of both the crystalline and amorphous phases. The weight ratio of the ZnO crystals to each crystal was calculated using the Rietveld refinement method. SEM images were obtained using the AURIGA system (Zeiss). Solid-state ^{31}P MAS-NMR spectra were acquired using a Bruker AVANCE II^+ 400 MHz NMR system (KBSI Seoul Western Center). Raman spectra were recorded with an Ar-ion laser beam at an excitation wavelength of 514 nm using a LabRAM Arimis instrument (Horiba Jobin Yvon). Elemental analyses were performed using a Flash 2000 organic elemental analyzer (Thermo Scientific). The ex situ XPS measurements were carried out with a monochromatic Al Kα source (1486.6 eV) at 12 kV and 3 mA using K-Alpha+ (Thermo Fisher Scientific). The samples were mounted on a sample holder in an Ar-filled glove box and transferred into the XPS equipment without any exposure to air.

4.3. Electrochemical characterization

The ionic conductivities were measured using the AC impedance method with Ti|SE|Ti symmetric cells. Pellets with a diameter of 6 mm were prepared at 370 MPa. The EIS data were collected using a VMP3 (Bio-Logic) instrument with an amplitude of 100 mV and a frequency range of 10^{-7} MHz. Electronic conductivities of SEs were determined through direct current polarization measurements carried out on pellets with applied voltages of 0.3, 0.5, 0.7, and 1.0 V, each for 30 min. To determine the ionic conductivity of F-LPSCl, tri-layer symmetric cells of (Li|LPSCl (200 mg)|Li) and five-layer symmetric cells (Li|LPSCl (100 mg)|F-LPSCl (70 mg)|LPSCl (100 mg)|Li) were fabricated. The ionic conductivity was obtained by subtracting the resistance of the Li|LPSCl|Li cell from that of the Li|LPSCl|F-LPSCl|LPSCl|Li [50]. Cell resistances were also measured using CV at a scan rate of 0.1 mV s^{-1}, and the obtained results were supported by EIS measurements. $LiNbO_3$-coated NCM powders were utilized in this study. The composite electrodes were prepared by mixing NCM, SE, and Super C65 in a weight ratio of 70:30:3 using a mortar and pestle. As a counter/reference electrode, $Li_{0.5}In$ (nominal composition) powder was prepared by mixing Li powder (FMC Lithium Corp.) and In powder (99%, Sigma-Aldrich). Cell assemblies were carried out in a poly(aryl-ether-ether-ketone) mold with a diameter of 13 mm and two Ti rods as the current collectors. The SE powders (150 mg) were pre-pelletized, after which the as-prepared NCM electrode (15 mg) and the Li-In electrode (75 mg) were placed on each side of the SE layer. Then, the assembled cells were pressed at 370 MPa. All NCM||Li-In cells were cycled between 3.0 and 4.3 V (vs. Li/Li^+) at 30 °C. To conduct CV measurements, SE-C||Li-In cells were fabricated. An SE and Super C65 mixture with a weight ratio of 10:1 was used as the working electrode. The LPSCl layer served as the separating SE layer, whereas the Li-In electrode acted as the counter/reference electrode.

CRediT authorship contribution statement

Boyeong Jang: Conceptualization, Data curation, Methodology, Investigation, Writing – original draft. **Jehoon Woo:** Conceptualization, Methodology, Investigation, Writing – original draft. **Yong Bae Song:** Investigation, Methodology. **Hiram Kwak:** Formal analysis, Investigation. **Juhyoun Park:** Formal analysis, Investigation. **Jong Seok Kim:** Formal analysis, Investigation. **Haechannara Lim:** Investigation. **Yoon Seok Jung:** Conceptualization, Supervision, Writing – review & editing.

Declaration of Competing Interest

The authors declare that they have no known competing financial interests or personal relationships that could have appeared to influence the work reported in this paper.

Acknowledgements

This work was supported by the National Research Foundation of Korea (NRF) funded by the Ministry of Science, ICT & Future Planning (2022M3J1A1085397) and by the Technology Innovation Program (20007045) funded by the Ministry of Trade, Industry & Energy (MOTIE, Korea).

Supplementary materials

Supplementary material associated with this article can be found, in the online version, at doi:10.1016/j.ensm.2023.103154.

References

[1] J. Janek, W.G. Zeier, A solid future for battery development, Nat. Energy 1 (2016) 16141, https://doi.org/10.1038/nenergy.2016.141.

[2] A. Manthiram, X. Yu, S. Wang, Lithium battery chemistries enabled by solid-state electrolytes, Nat. Rev. Mater. 2 (2017) 16103, https://doi.org/10.1038/natrevmats.2016.103.

[3] Z. Zhang, Y. Shao, B. Lotsch, Y.-S. Hu, H. Li, J. Janek, L.F. Nazar, C.-W. Nan, J. Maier, M. Armand;, et al., New horizons for inorganic solid state ion conductors, Energy Environ. Sci. 11 (2018) 1945–1976, https://doi.org/10.1039/C8EE01053F.

[4] T. Famprikis, P. Canepa, J.A. Dawson, M.S. Islam, C. Masquelier, Fundamentals of inorganic solid-state electrolytes for batteries, Nat. Mater. 18 (2019) 1278–1291, https://doi.org/10.1038/s41563-019-0431-3.

[5] R. Chen, Q. Li, X. Yu, L. Chen, H. Li, Approaching practically accessible solid-state batteries: stability issues related to solid electrolytes and interfaces, Chem. Rev. 120 (2020) 6820–6877, https://doi.org/10.1021/acs.chemrev.9b00268.

[6] Y. Kato, S. Hori, T. Saito, K. Suzuki, M. Hirayama, A. Mitsui, M. Yonemura, H. Iba, R. Kanno, High-power all-solid-state batteries using sulfide superionic conductors, Nat. Energy 1 (2016) 16030, https://doi.org/10.1038/nenergy.2016.30.

[7] Q. Zhang, D. Cao, Y. Ma, A. Natan, P. Aurora, H. Zhu, Sulfide-based solid-state electrolytes: synthesis, stability, and potential for all-solid-state batteries, Adv. Mater. 31 (2019), 1901131, https://doi.org/10.1002/adma.201901131.

[8] H. Kwak, S. Wang, J. Park, Y. Liu, K.T. Kim, Y. Choi, Y. Mo, Y.S. Jung, Emerging halide superionic conductors for all-solid-state batteries: design, synthesis, and practical applications, ACS Energy Lett 7 (2022) 1776–1805, https://doi.org/10.1021/acsenergylett.2c00438.

[9] Y.-G. Lee, S. Fujiki, C. Jung, N. Suzuki, N. Yashiro, R. Omoda, D.-S. Ko, T. Shiratsuchi, T. Sugimoto, S. Ryu;, et al., High-energy long-cycling all-solid-state lithium metal batteries enabled by silver–carbon composite anodes, Nat. Energy 5 (2020) 299–308, https://doi.org/10.1038/s41560-020-0575-z.

[10] S. Chen, D. Xie, G. Liu, J.P. Mwizerwa, Q. Zhang, Y. Zhao, X. Xu, X. Yao, Sulfide solid electrolytes for all-solid-state lithium batteries: structure, conductivity, stability and application, Energy Storage Mater 14 (2018) 58–74, https://doi.org/10.1016/j.ensm.2018.02.020.

[11] K.H. Park, Q. Bai, D.H. Kim, D.Y. Oh, Y. Zhu, Y. Mo, Y.S. Jung, Design strategies, practical considerations, and new solution processes of sulfide solid electrolytes for all-solid-state batteries, Adv. Energy Mater. 8 (2018), 1800035, https://doi.org/10.1002/aenm.201800035.

[12] A. Miura, N.C. Rosero-Navarro, A. Sakuda, K. Tadanaga, N.H.H. Phuc, A. Matsuda, N. Machida, A. Hayashi, M. Tatsumisago, Liquid-phase syntheses of sulfide electrolytes for all-solid-state lithium battery, Nat. Rev. Chem. 3 (2019) 189–198, https://doi.org/10.1038/s41570-019-0078-2.

[13] H. Kwak, J.-S. Kim, D. Han, J.S. Kim, J. Park, G. Kwon, S.-M. Bak, U. Heo, C. Park, H.-W. Lee;, et al., Boosting the interfacial superionic conduction of halide solid electrolytes for all-solid-state batteries, Nat. Commun. 14 (2023) 2459, https://doi.org/10.1038/s41467-023-38037-z.

[14] Y.B. Song, K.H. Baeck, H. Kwak, H. Lim, Y.S. Jung, Dimensional strategies for bridging the research gap between lab-scale and potentially practical all-solid-state batteries: the role of sulfide solid electrolyte films, Adv. Energy Mater. 13 (2023), 2301142, https://doi.org/10.1002/aenm.202301142.

[15] B. Tao, C. Ren, H. Li, B. Liu, X. Jia, X. Dong, S. Zhang, H. Chang, Thio-/LISICON and LGPS-type solid electrolytes for all-solid-state lithium-ion batteries, Adv. Funct. Mater. 32 (2022), 2203551, https://doi.org/10.1002/adfm.202203551.

[16] L. Duchêne, A. Remhof, H. Hagemann, C. Battaglia, Status and prospects of hydroborate electrolytes for all-solid-state batteries, Energy Storage Mater 25 (2020) 782–794, https://doi.org/10.1016/j.ensm.2019.08.032.

[17] H.-J. Deiseroth, S.-T. Kong, H. Eckert, J. Vannahme, C. Reiner, T. Zaiß, M. Schlosser, Li6PS5X: a class of crystalline li-rich solids with an unusually high Li + mobility, Angew. Chem. Int. Ed. 47 (2008) 755–758, https://doi.org/10.1002/anie.200703900.

[18] S. Yubuchi, M. Uematsu, C. Hotehama, A. Sakuda, A. Hayashi, M. Tatsumisago, An argyrodite sulfide-based superionic conductor synthesized by a liquid-phase technique with tetrahydrofuran and ethanol, J. Mater. Chem. A 7 (2019) 558–566, https://doi.org/10.1039/C8TA09477B.

[19] L. Zhou, K.-H. Park, X. Sun, F. Lalère, T. Adermann, P. Hartmann, L.F. Nazar, Solvent-engineered design of Argyrodite Li6PS5X (X = Cl, Br, I) solid electrolytes with high ionic conductivity, ACS Energy Lett 4 (2019) 265–270, https://doi.org/10.1021/acsenergylett.8b01997.

[20] P. Adeli, J.D. Bazak, K.H. Park, I. Kochetkov, A. Huq, G.R. Goward, L.F. Nazar, Boosting solid-state diffusivity and conductivity in lithium superionic argyrodites by halide substitution, Angew. Chem. Int. Ed. 58 (2019) 8681–8686, https://doi.org/10.1002/anie.201814222.

[21] Y.B. Song, D.H. Kim, H. Kwak, D. Han, S. Kang, J.H. Lee, S.-M. Bak, K.-W. Nam, H.-W. Lee, Y.S. Jung, Tailoring solution-processable Li Argyrodites $Li_{6+x}P_{1-x}M_xS_5I$ (M = Ge, Sn) and their microstructural evolution revealed by Cryo-TEM for all-solid-state batteries, Nano Lett 20 (2020) 4337–4345, https://doi.org/10.1021/acs.nanolett.0c01028.

[22] L. Zhou, N. Minafra, W.G. Zeier, L.F. Nazar, Innovative approaches to Li-Argyrodite solid electrolytes for all-solid-state lithium batteries, Acc. Chem. Res. 54 (2021) 2717–2728, https://doi.org/10.1021/acs.accounts.0c00874.

[23] D.H. Kim, H.A. Lee, Y.B. Song, J.W. Park, S.-M. Lee, Y.S. Jung, Sheet-type Li6PS5Cl-infiltrated Si anodes fabricated by solution process for all-solid-state lithium-ion batteries, J. Power Sources 426 (2019) 143–150, https://doi.org/10.1016/j.jpowsour.2019.04.028.

[24] J. Lau, R.H. DeBlock, D.M. Butts, D.S. Ashby, C.S. Choi, B.S. Dunn, Sulfide solid electrolytes for lithium battery applications, Adv. Energy Mater. 8 (2018), 1800933, https://doi.org/10.1002/aenm.201800933.

[25] Z. Liu, W. Fu, E.A. Payzant, X. Yu, Z. Wu, N.J. Dudney, J. Kiggans, K. Hong, A. J. Rondinone, C. Liang, Anomalous high ionic conductivity of nanoporous β-Li_3PS_4, J. Am. Chem. Soc. 135 (2013) 975–978, https://doi.org/10.1021/ja3110895.

[26] H.-D. Lim, X. Yue, X. Xing, V. Petrova, M. Gonzalez, H. Liu, P. Liu, Designing solution chemistries for the low-temperature synthesis of sulfide-based solid electrolytes, J. Mater. Chem. A 6 (2018) 7370–7374, https://doi.org/10.1039/C8TA01800F.

[27] H. Wang, Z.D. Hood, Y. Xia, C. Liang, Fabrication of ultrathin solid electrolyte membranes of β-Li_3PS_4 nanoflakes by evaporation-induced self-assembly for all-solid-state batteries, J. Mater. Chem. A 4 (2016) 8091–8096, https://doi.org/10.1039/C6TA02294D.

[28] M. Calpa, N.C. Rosero-Navarro, A. Miura, K. Tadanaga, Instantaneous preparation of high lithium-ion conducting sulfide solid electrolyte $Li_7P_3S_{11}$ by a liquid phase process, RSC Adv 7 (2017) 46499–46504, https://doi.org/10.1039/C7RA09081A.

[29] S. Ohsaki, T. Yano, A. Hatada, H. Nakamura, S. Watano, Size control of sulfide-based solid electrolyte particles through liquid-phase synthesis, Powder Technol 387 (2021) 415–420, https://doi.org/10.1016/j.powtec.2021.04.050.

[30] J. Woo, Y.B. Song, H. Kwak, S. Jun, B.Y. Jang, J. Park, K.T. Kim, C. Park, C. Lee, K.-H. Park;, et al., Liquid-phase synthesis of highly deformable and air-stable Sn-substituted Li_3PS_4 for all-solid-state batteries fabricated and operated under low pressures, Adv. Energy Mater. 13 (2023), 2203292, https://doi.org/10.1002/aenm.202203292.

[31] F. Marchini, B. Porcheron, G. Rousse, L. Albero Blanquer, L. Droguet, D. Foix, T. Koç, M. Deschamps, J.M. Tarascon, The hidden side of nanoporous β-Li_3PS_4 solid electrolyte, Adv. Energy Mater. 11 (2021), 2101111, https://doi.org/10.1002/aenm.202101111.

[32] N.H.H. Phuc, K. Morikawa, M. Totani, H. Muto, A. Matsuda, Chemical synthesis of Li_3PS_4 precursor suspension by liquid-phase shaking, Solid State Ion 285 (2016) 2–5, https://doi.org/10.1016/j.ssi.2015.11.019.

[33] J.E. Lee, K.-H. Park, J.C. Kim, T.-U. Wi, A.R. Ha, Y.B. Song, D.Y. Oh, J. Woo, S. H. Kweon, S.J. Yeom;, et al., Universal solution synthesis of sulfide solid electrolytes using alkahest for all-solid-state batteries, Adv. Mater. 34 (2022), 2200083, https://doi.org/10.1002/adma.202200083.

[34] T. Ito, S. Hori, M. Hirayama, R. Kanno, Liquid-phase synthesis of the $Li_{10}GeP_2S_{12}$-type phase in the Li–Si–P–S–Cl system, J. Mater. Chem. A 10 (2022) 14392–14398, https://doi.org/10.1039/D2TA02834D.

[35] S. Chida, A. Miura, N.C. Rosero-Navarro, M. Higuchi, N.H.H. Phuc, H. Muto, A. Matsuda, K. Tadanaga, Liquid-phase synthesis of Li_6PS_5Br using ultrasonication and application to cathode composite electrodes in all-solid-state batteries, Ceram. Int. 44 (2018) 742–746, https://doi.org/10.1016/j.ceramint.2017.09.241.

[36] S. Choi, J. Ann, J. Do, S. Lim, C. Park, D. Shin, Application of rod-like Li_6PS_5Cl directly synthesized by a liquid phase process to sheet-type electrodes for all-solid-state lithium batteries, J. Electrochem. Soc. 166 (2019) A5193, https://doi.org/10.1149/2.0301903jes.

[37] Y. Subramanian, R. Rajagopal, K.-S. Ryu, High ionic-conducting Li-argyrodites synthesized using a simple and economic liquid-phase approach and their application in all solid-state-lithium batteries, Scr. Mater. 204 (2021), 114129, https://doi.org/10.1016/j.scriptamat.2021.114129.

[38] R.F. Indrawan, H. Gamo, A. Nagai, A. Matsuda, Chemically understanding the liquid-phase synthesis of argyrodite solid electrolyte Li_6PS_5Cl with the highest ionic conductivity for all-solid-state batteries, Chem. Mater. 35 (2023) 2549–2558, https://doi.org/10.1021/acs.chemmater.2c03818.

[39] X. Hu, D. Zuo, S. Cheng, S. Chen, Y. Liu, W. Bao, S. Deng, S.J. Harris, J. Wan, Ultrafast materials synthesis and manufacturing techniques for emerging energy and environmental applications, Chem. Soc. Rev. 52 (2023) 1103–1128, https://doi.org/10.1039/D2CS00322H.

[40] Y. Yao, Z. Huang, P. Xie, S.D. Lacey, R.J. Jacob, H. Xie, F. Chen, A. Nie, T. Pu, M. Rehwoldt;, et al., Carbothermal shock synthesis of high-entropy-alloy nanoparticles, Science 359 (2018) 1489–1494, https://doi.org/10.1126/science.aan5412.

[41] J. Lu, S. Liu, J. Liu, G. Qian, D. Wang, X. Gong, Y. Deng, Y. Chen, Z. Wang, Millisecond conversion of photovoltaic silicon waste to binder-free high silicon content nanowires electrodes, Adv. Energy Mater. 11 (2021), 2102103, https://doi.org/10.1002/aenm.202102103.

[42] V.C. Wu, H.A. Evans, R. Giovine, M.B. Preefer, J. Ong, E. Yoshida, P.-E. Cabelguen, R.J. Clément, Rapid and energy-efficient synthesis of disordered rocksalt cathodes, Adv. Energy Mater. 13 (2023), 2203860, https://doi.org/10.1002/aenm.202203860.

[43] M. Oghbaei, O. Mirzaee, Microwave versus conventional sintering: a review of fundamentals, advantages and applications, J. Alloy. Compd. 494 (2010) 175–189, https://doi.org/10.1016/j.jallcom.2010.01.068.

[44] H.J. Kitchen, S.R. Vallance, J.L. Kennedy, N. Tapia-Ruiz, L. Carassiti, A. Harrison, A.G. Whittaker, T.D. Drysdale, S.W. Kingman, D.H. Gregory, Modern microwave methods in solid-state inorganic materials chemistry: from fundamentals to manufacturing, Chem. Rev. 114 (2014) 1170–1206, https://doi.org/10.1021/cr4002353.

[45] G. Zhong, C. Wang, R. Wang, W. Ping, S. Xu, H. Qiao, M. Cui, X. Wang, Y. Zhou, D. J. Kline;, et al., Rapid, high-temperature microwave soldering toward a high-performance cathode/electrolyte interface, Energy Storage Mater 30 (2020) 385–391, https://doi.org/10.1016/j.ensm.2020.05.015.

[46] S. Chen, L. Nie, X. Hu, Y. Zhang, Y. Zhang, Y. Yu, W. Liu, Ultrafast sintering for ceramic-based all-solid-state lithium-metal batteries, Adv. Mater. 34 (2022), 2200430, https://doi.org/10.1002/adma.202200430.

[47] C. Wang, W. Ping, Q. Bai, H. Cui, R. Hensleigh, R. Wang, A.H. Brozena, Z. Xu, J. Dai, Y. Pei;, et al., A general method to synthesize and sinter bulk ceramics in seconds, Science 368 (2020) 521–526, https://doi.org/10.1126/science.aaz7681.
[48] K. Suto, P. Bonnick, E. Nagai, K. Niitani, T.S. Arthur, J. Muldoon, Microwave-aided synthesis of lithium thiophosphate solid electrolyte, J. Mater. Chem. A 6 (2018) 21261–21265, https://doi.org/10.1039/C8TA08070D.
[49] G. Zhong, S. Xu, Q. Dong, X. Wang, L. Hu, Rapid, universal surface engineering of carbon materials via microwave-induced carbothermal shock, Adv. Funct. Mater. 31 (2021), 2010968, https://doi.org/10.1002/adfm.202010968.
[50] K. Nagao, Y. Nagata, A. Sakuda, A. Hayashi, M. Deguchi, C. Hotehama, H. Tsukasaki, S. Mori, Y. Orikasa, K. Yamamoto;, et al., A reversible oxygen redox reaction in bulk-type all-solid-state batteries, Sci. Adv. 6 (2020) eaax7236, https://doi.org/10.1126/sciadv.aax7236.
[51] C. Dietrich, D.A. Weber, S.J. Sedlmaier, S. Indris, S.P. Culver, D. Walter, J. Janek, W.G. Zeier, Lithium ion conductivity in Li_2S–P_2S_5 glasses – building units and local structure evolution during the crystallization of superionic conductors Li_3PS_4, $Li_7P_3S_{11}$ and $Li_4P_2S_7$, J. Mater. Chem. A 5 (2017) 18111–18119, https://doi.org/10.1039/C7TA06067J.
[52] Z. Liu, T. Zinkevich, S. Indris, X. He, J. Liu, W. Xu, J. Bai, S. Xiong, Y. Mo, H. Chen, $Li_{15}P_4S_{16}Cl_3$, a lithium chlorothiophosphate as a solid-state ionic conductor, Inorg. Chem. 59 (2020) 226–234, https://doi.org/10.1021/acs.inorgchem.9b01751.
[53] G.O. Hartley, L. Jin, B.J. Bergner, D.S. Jolly, G.J. Rees, S. Zekoll, Z. Ning, A.T. R. Pateman, C. Holc, P. Adamson;, et al., Is nitrogen present in Li_3N·P_2S_5 solid electrolytes produced by ball milling? Chem. Mater. 31 (2019) 9993–10001, https://doi.org/10.1021/acs.chemmater.9b01853.
[54] E.D. West, The heat capacity of sulfur from 25 to 450, the heats and temperatures of transition and fusion1, 2, J. Am. Chem. Soc. 81 (1959) 29–37, https://doi.org/10.1021/ja01510a008.
[55] Y.-S. Kim, S.H. Jeon, W. Cho, K. Kim, J. Yu, J. Yi, G. Jeong, K.-H. Park, Surficial sulfur loss of jet-milled Li6PS5Cl powder under mild-temperature heat treatment, ACS. Appl. Energy Mater 5 (2022) 15442–15451, https://doi.org/10.1021/acsaem.2c03040.
[56] A.C. Ferrari, J. Robertson, Interpretation of Raman spectra of disordered and amorphous carbon, Phys. Rev. B 61 (2000) 14095–14107, https://doi.org/10.1103/PhysRevB.61.14095.
[57] J. Auvergniot, A. Cassel, J.-B. Ledeuil, V. Viallet, V. Seznec, R. Dedryvère, Interface stability of argyrodite Li_6PS_5Cl toward $LiCoO_2$, $LiNi_{1/3}Co_{1/3}Mn_{1/3}O_2$, and $LiMn_2O_4$ in bulk all-solid-state batteries, Chem. Mater. 29 (2017) 3883–3890, https://doi.org/10.1021/acs.chemmater.6b04990.
[58] T. Hakari, M. Deguchi, K. Mitsuhara, T. Ohta, K. Saito, Y. Orikasa, Y. Uchimoto, Y. Kowada, A. Hayashi, M. Tatsumisago, Structural and electronic-state changes of a sulfide solid electrolyte during the Li deinsertion–insertion processes, Chem. Mater. 29 (2017) 4768–4774, https://doi.org/10.1021/acs.chemmater.7b00551.
[59] S.H. Jung, K. Oh, Y.J. Nam, D.Y. Oh, P. Brüner, K. Kang, Y.S. Jung, Li_3BO_3–Li_2CO_3: rationally designed buffering phase for sulfide all-solid-state Li-Ion batteries, Chem. Mater. 30 (2018) 8190–8200, https://doi.org/10.1021/acs.chemmater.8b03321.
[60] S.H. Jung, U.-H. Kim, J.-H. Kim, S. Jun, C.S. Yoon, Y.S. Jung, Y.-K. Sun, Ni-Rich layered cathode materials with electrochemo-mechanically compliant microstructures for all-solid-state Li batteries, Adv. Energy Mater. 10 (2020), 1903360, https://doi.org/10.1002/aenm.201903360.
[61] Y. Han, S.H. Jung, H. Kwak, S. Jun, H.H. Kwak, J.H. Lee, S.-T. Hong, Y.S. Jung, Single- or poly-crystalline Ni-rich layered cathode, sulfide or halide solid electrolyte: which will be the winners for all-solid-state batteries? Adv. Energy Mater. 11 (2021), 2100126 https://doi.org/10.1002/aenm.202100126.
[62] J.S. Kim, S. Jung, H. Kwak, Y. Han, S. Kim, J. Lim, Y.M. Lee, Y.S. Jung, Synergistic halide-sulfide hybrid solid electrolytes for Ni-rich cathodes design guided by digital twin for all-solid-State Li batteries, Energy Storage Mater 55 (2023) 193–204, https://doi.org/10.1016/j.ensm.2022.11.038.
[63] J. Hoffmann, M. Nüchter, B. Ondruschka, P. Wasserscheid, Ionic liquids and their heating behaviour during microwave irradiation – a state of the art report and challenge to assessment, Green Chem 5 (2003) 296–299, https://doi.org/10.1039/B212533A.